Advances in Mechanical and Materials Engineering

Volume 40, 2023, Pages 63-78
https://doi.org/10.7862/rm.2023.8

THE FACULTY OF MECHANICAL ENGINEERING AND AERONAUTICS
RZESZOW UNIVERSITY OF TECHNOLOGY

Original Research

Crystal Plasticity Elastic-Plastic Rate-Independent Numerical Analyses of Pollycrystalline Materials

Marta Wójcik [1,*], Andrzej Skrzat [1], Feliks Stachowicz [1], Emil Spišák [2]

[1] Department of Materials Forming and Processing, Faculty of Mechanical Engineering and Aeronautics, Rzeszow University of Technology, 8 Powstańców Warszawy Ave., 35-959 Rzeszów, Poland
[2] Department of Technology, Materials and Computer Supported Production, Faculty of Mechanical Engineering, Technical University of Košice, 74 Mäsiarska St., 040 01 Košice, Slovakia

* Correspondence: m.wojcik@prz.edu.pl, tel.: +48 17 865 15 07

Received: 19 January 2023 / Accepted: 11 February 2023 / Published online: 17 February 2023

Abstract

Macroscopic analyses of plastic forming processes give only the overall description of the problem without the consideration of mechanisms of plastic deformation and the microstructure evolution. For the consideration of these processes, numerical simulations within crystal plasticity include the change of texture, anisotropy, and strain hardening of the material are used. In this paper, a crystal plasticity rate-independent model proposed by Anand and Kothari is applied for numerical analyses of polycrystalline materials. The slip was considered as the main mechanism of the plastic deformation. Basic constitutive equations of crystal plasticity for large deformation theories are presented. The selected results of elastic-plastic problems obtained using both macro- and micro- scales software for the explicit and implicit integration are featured here. The heterogeneous distribution of strain and stress in different grains are obtained, which is associated with the various crystal orientation. The crystal plasticity modelling of materials subject to plastic deformation involves not only the information about the change of a material's shape in a macro-scale, but also describes the phenomena occurring in material in a micro-scale.

Keywords: crystal plasticity, polycrystalline materials, plastic deformation, CPFEM, dislocation slip

1. Introduction

Numerical analyses of elastic-plastic problems of materials forming and processing can be solved on macroscopic level using the classical plasticity theory or on the microscopic one using crystal plasticity. This first approach describes the behaviour of materials under loading only in a macroscopic scale without taking into consideration its micromechanical changes. In such macroscopic analyses, a variety of models, e.g. Prager, Ziegler, Johnson-Cook, Ohno-Wang, Frederick-Armstrong, and Chaboche ones are commonly applied (Buljak et al., 2021; Genna, 1993; Remache et al., 2020; Chen et al., 2005; Schäfer, 2019; Sajjad et al., 2019). Material processing analyses including only the macroscopic behaviour of materials under cyclic loading were tested by authors in the past. Wójcik and Skrzat (2020) applied the Frederick-Armstrong model in order to predict the stress-strain response of a material subject to the cyclic loading test. Authors were also testing the application of both Frederick-Armstrong and Chaboche models in numerical analyses of the KOBO extrusion (Wójcik & Skrzat, 2022b; Wójcik & Skrzat, 2021). Although the good convergence between experimental and numerical results is obtained, only the macroscopic response of the material was considered. It gives the incomplete description of the material behavior, especially in the case of large deformation processes, Severe Plastic Deformation (SPD) processes in which the significant refinement of a microstructure is a very important feature.

The crystal plasticity (CP) theory presents a full explanation of a material plastic deformation under loading and includes both the change of the material shape in a macro scale, as well as, its microstructure evolution and grains anisotropy (Men & Meng, 2022). The CP models link different scales of the problem considered – from macro- to micro- and to nano- levels. The CP theory has been developed as a

useful tool to describe the mechanical response of polycrystalline materials on all scales from single crystals to whole engineering parts in last thirty years (Dabiri et al., 2018).

In the CP approach, materials are considered as polycrystals with a large number of grains in which each grain has a specific crystallographic orientation. The single crystal has the three-dimensional arrangement of atoms - FCC (face centered cubic), BCC (body centered cubic) or HCP (hexagonal close packed) (Ramos et al., 2020). The level of the plastic deformation in a polycrystalline material varies from one crystal to another, which depends on, e.g. the orientation, geometry, neighboring crystals and loading conditions (Yang & Park, 2003).

Contrary to the classical theory of plasticity, the CP takes into consideration the mechanisms of plastic deformation in materials – mainly slip and twinning. The CP models based on the slip are well-known and developed in the CP theory (Bridier et al., 2009; Messner et al., 2017; Alankar et al., 2011). Models assuming twinning are in the intensive development at present. Liu et al. (2021) proposed the coupled crystal plasticity finite element-phase field model with kinetics-controlled twinning. Abdolvand et al. (2011) developed the crystal plasticity model assuming the twinning reorientation. The numerical modelling of twinning-induced plasticity using crystal plasticity finite element method (CPFEM) is described in by Khan et al. (2016). Apart from the heterogeneity of plastic strain in crystalline materials caused by the anisotropy of grains, a lot of CP models available assume some simplifications. In the Taylor model, all grains have the same strain state common to the global strain (Pramanik, 2021). Every grain is deformed in the same way as the representative volume element (RVE) here. The Sachs model assumes the same stress state for all grains which is the same as the global stress state of the material (Romanova, 2022). It results in the discontinuity of displacements. In the self-consistent model, every grain is considered as an ellipsoidal heterogeneity placed in a uniform space representing the polycrystalline structure (Li et al., 2021).

Apart from popular models, there are also new approaches in order to simulate the behaviour of a material under loading based on the CP theory. The microstructure-based CP model in order to evaluate the shear deformation behavior of a material under cyclic load is described by Yang et al. (2022). The new twinning-induced crystal plasticity model in terms of the thermomechanical framework and with a new integration method, is developed by Khan and Alfozan (2019). The fully implicit integration procedure for a twinning-induced plasticity model based on the CP approach is also presented by Khan et al. (2022). The propositions of other new models using the CP theory in order to simulate the behaviour of material in a microscopic scale are also available in literature (Li et al., 2022; Ibragimova et al., 2021; Li et al., 2020; Jeong & Voyiadjis, 2022).

The plastic deformation due to the dislocation slip was considered in this paper. Anisotropic slip occurs only in selected directions and in selected crystalline planes which define slip systems (Nguyen, 2021). Additionally, the dislocation slip does not change the crystalline orientation of a material. All atoms in a lattice maintain the same distance with each other, therefore (Faul, 2021). Polycrystalline structures have a different number of slip systems determined by ***n*** and ***m*** vectors which describe the normal to the slip plane and the slip direction, respectively. For FCC structure considered here, four sets of slip planes {111} and three close packed slip directions <110> in each plane are determined, which gives a combination of twelve slip systems (Weinberger, 2013). The plastic deformation caused by the slip occurs more easily in crystals which have higher number of the slip systems and which are located more favorably against the a load direction (Wójcik & Skrzat, 2022a).

The activation of slip systems is described by Schmid's law. The yielding in a crystal takes place when the resolved shear stress (τ^{α}) of a selected slip system exceeds its critical resolved shear stress - τ_{CRSS} (Eq. 1) (Mlikota & Schmauder, 2018).

$$\tau^{\alpha} = \sigma cos\phi cos\lambda > \tau_{CRSS} \tag{1}$$

where: σ is a tensile stress, λ is an angle between tensile axis and the slip direction and ϕ is an angle between tensile angle and the slip plane normal. The $cos\varphi cos\lambda$ coefficient defines the Schmid factor.

Numerical elastic-plastic analyses of a copper alloy subjected to simple tension tests are presented here. The simulations were done for different shapes of samples. The material was modelled as a polycrystalline anisotropic material with the random distribution of grains. The CP analyses were performed using open -source NEPPER and FEPX, and commercial Simulia Abaqus softwares. The Anand and Kothari approach was applied here. It is a relatively simple, effective and efficient numerically model in order to calculate the stress increment. The main advantage of the method is that the Anand and Kothari procedure presents the way to choose the slip systems which is a long-lasting problem of the rate-independent CP theory. Additionally, the CP approach developed by Anand and Kothari is

implemented in the PRISMS commercial software which can be used as a reference solution in order to check the correctness of a solution. The results obtained presents the potential of CP as an effective numerical approach for solving engineering problems, including modeling of materials forming processes characterized by the large plastic deformation. The micromechanical analyses using CP theory give a more complete description of the material behavior under loading than classical macro-mechanical approaches.

2. Constitutive equations of Crystal Plasticity theory

The rate-independent CP constitutive model for a single crystal FCC structure developed by Anand & Kothari (1996) is used in this paper. Based on assumption of deformation decomposition into elastic and plastic parts CP constitutive equations are as follows:

1) Multiplicative decomposition of deformation gradient $\boldsymbol{F}$ into elastic $\boldsymbol{F}^e$ and plastic components $\boldsymbol{F}^p$ is the following (Eq. 2):

$$\boldsymbol{F} = \boldsymbol{F}^e \boldsymbol{F}^p \tag{2}$$

Elastic part includes the information about rotation and stretching, plastic part influences on plastic shearing on crystallographic slip systems and defines dislocations (Fig. 1) (Paudel et al., 2021).

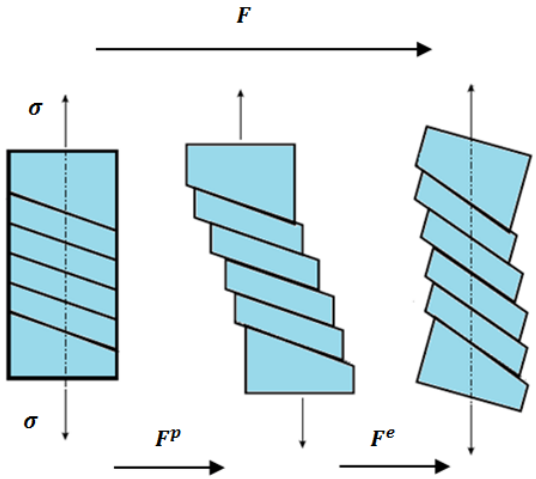

Fig. 1. Explanation of elastic and plastic parts of the deformation gradient tensor

2) The macroscopic velocity gradient $\boldsymbol{L}$ is decomposed additively into elastic and plastic parts (Eq. 3), as well as into symmetric and antisymmetric ones (Eq. 4):

$$\boldsymbol{L} = \boldsymbol{L}^e + \boldsymbol{L}^p = \dot{\boldsymbol{F}}^e(\boldsymbol{F}^{\mathrm{e}})^{-1} + \boldsymbol{F}^e\dot{\boldsymbol{F}}^p(\boldsymbol{F}^p)^{-1}(\boldsymbol{F}^e)^{-1} \tag{3}$$

$$\boldsymbol{L} = \boldsymbol{D} + \boldsymbol{\Omega} \tag{4}$$

where: $\mathbf{L}^{\mathrm{e}}$ and $\mathbf{L}^{\mathrm{p}}$ are elastic and plastic velocity gradient tensors, respectively; $\boldsymbol{D}$ is symmetric deformation velocity tensor and $\boldsymbol{\Omega}$ is an antisymmetric spin (Eq. 5-6). Similarly to tensor $\boldsymbol{L}$, tensors $\boldsymbol{D}$ and $\boldsymbol{\Omega}$ are additively decomposed into elastic and plastic parts in line with Eq. 7-8:

$$\boldsymbol{D} = sym(\boldsymbol{L}) = \frac{1}{2}(\boldsymbol{L} + \boldsymbol{L}^T) \tag{5}$$

$$\boldsymbol{\Omega} = asym(\boldsymbol{L}) = \frac{1}{2}(\boldsymbol{L} - \boldsymbol{L}^T) \tag{6}$$

$$\boldsymbol{D} = \boldsymbol{D}^e + \boldsymbol{D}^p \tag{7}$$

$$\boldsymbol{\Omega} = \boldsymbol{\Omega}^e + \boldsymbol{\Omega}^p \tag{8}$$

3) On the basis of the polar decomposition, the elastic part of the deformation gradient might be expressed as a multiplication of a rigid body tensor $\boldsymbol{R}^e$ and the right stretching tensor $\boldsymbol{U}^e$ (Eq. 9). Using the $\boldsymbol{R}$ tensor, the elastic part of a spin might be written as (Eq. 10):

$$\boldsymbol{F}^e = \boldsymbol{R}^e \boldsymbol{U}^e \tag{9}$$

$$\boldsymbol{\Omega}^{\boldsymbol{e}} = \boldsymbol{R}^{\boldsymbol{e}} \cdot \dot{\boldsymbol{R}}^{eT} \tag{10}$$

4) The macroscopic plastic velocity gradient links different scales of the problem considered (macro- and micro-) (Men & Meng, 2022; Ryś et al., 2022). It might be expressed as the superposition of shear deformation caused by the crystallographic slip (Eq. 11):

$$\boldsymbol{L}^p = \sum_{\alpha=1}^{n} \dot{\gamma}^{\alpha} \boldsymbol{S}^{\alpha} \tag{11}$$

where: $\dot{\gamma}^{\alpha}$ is the shearing rate on the α slip system, n is a total number of slip systems and $\boldsymbol{S}^{\alpha}$ is the Schmid tensor for the slip system α defined as follows (Eq. 12):

$$\boldsymbol{S}^{\alpha} = \boldsymbol{m}^{\alpha} \otimes \boldsymbol{n}^{\alpha} \tag{12}$$

where: $\boldsymbol{m}^{\alpha}$ is the slip direction and $\boldsymbol{n}^{\alpha}$ defines the slip plane normal, as well as, $\boldsymbol{m}^{\alpha}$ and $\boldsymbol{n}^{\alpha}$ are orthogonal (Nibur & Bahr, 2003). Assuming the microscopic level, the plastic deformation velocity gradient $\boldsymbol{D}^{\boldsymbol{p}}$ and the plastic spin $\boldsymbol{\Omega}^{\boldsymbol{p}}$ tensors are expressed in line with the following equations (Eq. 13-14) (Deng, 2014).

$$\boldsymbol{D}^p = \frac{1}{2}(\boldsymbol{L}^p + \boldsymbol{L}^{pT}) = \sum_{\alpha=1}^{n} \boldsymbol{p}^{\alpha} \cdot \dot{\gamma}^{\alpha} \tag{13}$$

$$\boldsymbol{\Omega}^p = \frac{1}{2}(\boldsymbol{L}^p - \boldsymbol{L}^{pT}) = \sum_{\alpha=1}^{n} \boldsymbol{\omega}^{\alpha} \cdot \dot{\gamma}^{\alpha} \tag{14}$$

where: $\boldsymbol{p}^{\alpha}$ and $\boldsymbol{\omega}^{\alpha}$ are symmetric and asymmetric tensors defining the Schmid tensor on the α slip system defined as follows (Eq. 15-16).

$$\boldsymbol{p}^{\alpha} = \frac{1}{2}(\boldsymbol{n}^{\alpha} \otimes \boldsymbol{m}^{\alpha} + \boldsymbol{m}^{\alpha} \otimes \boldsymbol{n}^{\alpha}) \tag{15}$$

$$\boldsymbol{\omega}^{\alpha} = \frac{1}{2}(\boldsymbol{n}^{\alpha} \otimes \boldsymbol{m}^{\alpha} - \boldsymbol{m}^{\alpha} \otimes \boldsymbol{n}^{\alpha}) \tag{16}$$

5) The resolved shear stress which causes the shear on a given crystallographic plane in a given crystallographic direction is defined as (Eq. 17) (Frydrych & Kowalczyk-Gajewska, 2016):

$$\tau^{\alpha} = \boldsymbol{\sigma} : \boldsymbol{S}^{\alpha} = \boldsymbol{\sigma} : (\boldsymbol{m}^{\alpha} \otimes \boldsymbol{n}^{\alpha}) \tag{17}$$

6) Based on Schmid's law, the CP hardening model of polycrystalline material and shear rate $\dot{\gamma}^{\alpha}$ for the α slip system evaluate as follows (Eq. 18):

$$\dot{\gamma}^{\alpha} = \dot{\gamma}_0 \left(\frac{|\tau^{\alpha}|}{g^{\alpha}}\right)^k sgn(\tau^{\alpha}) \tag{18}$$

where: $\dot{\gamma}_0$ is the reference shear strain rate on the α slip system, τ^{α} is the resolved shear stress on the α slip system, k is the rate sensitivity coefficient, g^{α} is the critical shear stress on the α activated slip system to govern the isotropic hardening of the crystal and sgn is a signum function. For a rate-independent CP, $k \to \infty$ (Yaghoobi et al., 2019).

7) The shear rate $\dot{\gamma}^{\alpha}$ which consists of the effect of a backstress related with the kinematic hardening is written by the following (Eq. 19):

$$\dot{\gamma}^{\alpha} = \dot{\gamma}_0 sgn(\tau^{\alpha} - x^{\alpha}) \left(\frac{|\tau^{\alpha} - x^{\alpha}|}{g^{\alpha}}\right)^k \tag{19}$$

where: x^{α} is a backstress describing the nonlinear kinematic (directional) hardening of the crystal on the α slip system.

8) The evolution of a slip resistance ($\dot{g}^{\alpha}$) for the α slip system is described as follows (Eq. 20):

$$\dot{g}^{\alpha} = \sum_{\beta} h^{\alpha\beta}\dot{\gamma}^{\beta} \tag{20}$$

where: $h^{\alpha\beta}$ is a hardening modulus defining the variation of slip resistance for the α slip system due to the slip rate on β slip system and might be defined as a relationship assuming both hardening and recovery (Eq. 21) (Asaro & Needleman, 1985):

$$h^{\alpha\beta} = \begin{cases} h_0^{\beta}\left[1 - \frac{g^{\beta}}{g_s^{\beta}}\right]^{\alpha^{\beta}} & for\ \alpha = \beta \\ h_0^{\beta} q\left[1 - \frac{g^{\beta}}{g_s^{\beta}}\right]^{\alpha^{\beta}} & for\ \alpha \neq \beta \end{cases} \tag{21}$$

where: q is a latent hardening ratio, h_0^{β} is a hardening parameter for β slip system, g_s^{β} defines the slip resistance at hardening saturation for β slip system, and α^{β} is a material constant for β slip system defining the sensitivity of the hardening moduli to the slip resistance (Khan & Alfozan, 2019). It is assumed that $h^{\alpha\beta}$ is a self-hardening modulus for $\alpha = \beta$ or for $\alpha \neq \beta$, $h^{\alpha\beta}$ is a latent hardening one (Yaghoobi et al., 2019).

The Anand & Kothari model presented above indicates very good compatibility with the experimental data in most cases. Acar et al. (2017) obtained a very good convergence between the microstructure measured experimentally and achieved in simulations using the Anand and Kothari model for a titanium-aluminum alloy. The research of Balasubramanian & Anand (2002) also confirmed the very good agreement between numerical and experimental stress-strain response, strain-rate history and temperature-history effect for aluminum with the use of Anand and Kothari model.

3. Numerical integration of Crystal Plasticity constitutive equations

The numerical calculations of elastic-plastic problems based on the CP theory with the use of equations presented in Section 2 are time-consuming and complex. A lot of computation steps are required in such analyses and the calculations are done iteratively in a loop. These steps are shown in Fig. 2.

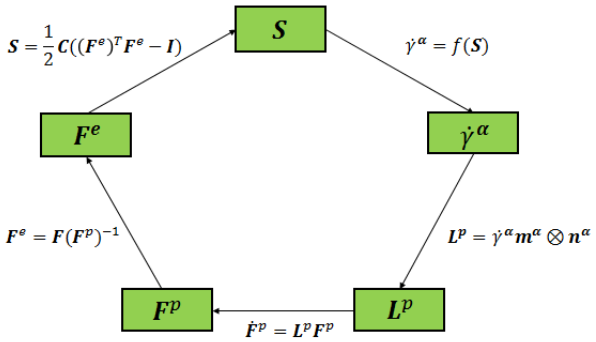

Fig. 2. Diagram showing the complexity of calculations using the CP theory

The implicit integration procedure of constitutive equations is presented here. Five state variables $\{\boldsymbol{F}(t), \boldsymbol{F}^e(t), \boldsymbol{F}^p(t), \boldsymbol{\sigma}(t)$ Cauchy stress and $g^{\alpha}(t)\}$ at initial time t undergo the incremental deformation, and then they are updated for the time $t_1 = t + \Delta t$. The given data are $\boldsymbol{F}(t)$, $\boldsymbol{F}(t_1)$, stress $\boldsymbol{S}(t)$, $g^{\alpha}(t)$ and time- independent parameters defining the slip system ($\boldsymbol{m}_0^{\alpha}$ and $\boldsymbol{n}_0^{\alpha}$). The $\boldsymbol{F}^p(t_1)$, $\boldsymbol{T}(t_1)$ and $g^{\alpha}(t_1)$, as well as the information about the orientation of the slip system, are calculated. Unfortunately, there are only five independent plastic strain components available (six plastic strain components are constrained by the incompressibility condition, while potentially twelve slip systems should be determined. In this research we use the integration procedure proposed by Anand and Kothari which is summarized as follows.

1) Firstly, the trial elastic strain $E^e(t_1)^{tr}$ is calculated in line with the Eq. 22-24.

$$\boldsymbol{F}^e(t_1)^{tr} = \boldsymbol{F}(t_1)\boldsymbol{F}^p(t_1) \tag{22}$$

$$\boldsymbol{C}^e(t_1)^{tr} = (\boldsymbol{F}^e(t_1)^{tr})^T \boldsymbol{F}^e(t_1)^{tr} \tag{23}$$

$$\boldsymbol{E}^e(t_1)^{tr} = \frac{1}{2}[\boldsymbol{C}^e(t_1)^{tr} - \boldsymbol{I}] \tag{24}$$

where: $\boldsymbol{C}^e$ is elastic right Cauchy-Green strain tensor and $\boldsymbol{I}$ is the identity matrix.

2) Based on the trial elastic strain the $\boldsymbol{S}^*(t_1)^{tr}$ trial stress tensor is determined (Eq. 25).

$$\boldsymbol{S}^*(t_1)^{tr} = \ell[\boldsymbol{E}^e(t_1)^{tr}] \tag{25}$$

where: ℓ *is* the fourth order elastic stiffness tensor.

3) The trial resolved shear stress $\tau^\alpha(t_1)^{tr}$ on each slip system expressed by the Schmid tensor is calculated as follows (Eq. 26-27):

$$\tau^\alpha(t_1)^{tr} = \boldsymbol{S}^*(t_1)^{tr} \cdot \boldsymbol{S}_0^\alpha \tag{26}$$

$$\boldsymbol{S}_0^\alpha = \boldsymbol{m}_0^\alpha \otimes \boldsymbol{n}_0^\alpha \tag{27}$$

In Eq. 26, $\boldsymbol{S}_0^\alpha$ Schmid tensor for α slip system is the same in both relaxed and undeformed configuration because plastic slip does not directly affect the crystallography of the underlying lattice (Faul, 2021).

4) Assuming some simplifications, the following relationship can be written as (Eq. 28):

$$sign[\tau^\alpha(t_1)^{tr}] = sign[\tau^\alpha(t_1)] \tag{28}$$

The determination of active slip systems and shear increments require long-lasting computations in rate-independent CP theory. The following approach for the determination of active and inactive slip systems based on the plasticity condition (Eq. 29) might be applied.

$$f^\alpha = |\tau^\alpha| - g^\alpha \tag{29}$$

According to the Kuhn-Tucker special consistency conditions, the slip system is inactive if $\dot{\gamma}_\alpha = 0$ and $|\tau^\alpha| < g^\alpha$ or if $|\tau^\alpha| = g^\alpha$ and the trial stress rate points to the inside of the yield surface. For active slip systems, $|\tau^\alpha| = g^\alpha$, $\dot{\gamma}_\alpha > 0$ and the trial stress rate points to the outside of the yield surface (Sundararaghavan & Zabaras, 2008). In order to determine the active slip systems and corresponding slip increments, the consistency condition in the form of linear equations (Eq. 30) is applied.

$$\sum_{\beta \epsilon A} A^{\alpha\beta} \dot{\gamma}^\beta = b^\alpha \tag{30}$$

in which: A is a set of potentially active slip systems and matrix $A^{\alpha\beta}$ defines potentially active slip systems. At the end of calculations, the size of $A^{\alpha\beta}$ matrix is reduced to m by m where m means the number of active slip systems. The search for active slip systems relies on the solving of the system of linear equations above (see Eq. 30) until all systems meet the requirement $\dot{\gamma}^\beta > 0$. If the system is inactive, it is removed from the set of active slip systems and the size of matrix A is reduced, therefore (Li et al., 2021).

5) Next the plastic deformation gradient $\boldsymbol{F^p}(t_1)$ at time t_1 is updated (Eq. 31).

$$\boldsymbol{F^p}(t_1) = \{\boldsymbol{I} + \sum_{\alpha=1}^{m} sign(\tau^\alpha(t_1)^{tr}) \Delta\gamma^\alpha \boldsymbol{S}_0^\alpha\} \boldsymbol{F}^p(t) \tag{31}$$

6) Then it is necessary to check if $det\boldsymbol{F^p}(t_1) = 1$. If this condition is not satisfied, $\boldsymbol{F^p}(t_1)$ is normalized as follows (Eq. 32).

$$\boldsymbol{F^p}(t_1) = [\det \boldsymbol{F}^p(t_1)]^{-1/3} \boldsymbol{F}^p(t_1) \tag{32}$$

7) In the further step, the elastic deformation gradient $\boldsymbol{F^e}(t_1)$ and stress tensor $\boldsymbol{S}^*(t_1)$ are computed (Eq. 33-34).

$$\boldsymbol{F^e}(t_1) = \boldsymbol{F}(t_1) \boldsymbol{F}^{p-1}(t_1) \tag{33}$$

$$\boldsymbol{S}^*(t_1) = \boldsymbol{S}^e(t_1)^{tr} - \sum_{\alpha=1}^{m} \{\Delta\gamma^\alpha sign(\tau^\alpha(t_1)^{tr})\} \ell[sym(\boldsymbol{C}^e(t_1)^{tr} \boldsymbol{S}_0^\alpha)] \tag{34}$$

8) At the end of the integration procedure, the $\boldsymbol{S}(t_1)$ and $g^{\alpha}(t_1)$ variables, as well as, parameters associated with the texture evolution - $\boldsymbol{m}_{t_1}^{\alpha}$ and $\boldsymbol{n}_{t_1}^{\alpha}$ are calculated (Eq. 35-38).

$$\boldsymbol{S}(t_1) = \boldsymbol{F}^e(t_1)\{[det\boldsymbol{F}^e(t_1)]^{-1}\boldsymbol{S}^*(t_1)\}\boldsymbol{F}^{e^T}(t_1) \tag{35}$$

$$g^{\alpha}(t_1) = g^{\alpha}(t) + \sum_{\beta=1}^{N} h^{\alpha\beta}\Delta\gamma^{\beta}\,, \quad \alpha = 1, \dots, N \tag{36}$$

$$\boldsymbol{m}_{t1}^{\alpha} = \boldsymbol{F}^e(t_1)\boldsymbol{m}_0^{\alpha} \tag{37}$$

$$\boldsymbol{n}_{t1}^{\alpha} = \boldsymbol{F}^e(t_1)\boldsymbol{n}_0^{\alpha} \tag{38}$$

The integration procedure presented above has been implemented by authors in the form of the user material subroutine in ABAQUS program. The same approach is also used in PRISMS open software, which can be applied in solving benchmark tests treated as reference solutions. It is worth noting that static procedure requires the Jacobian matrix for the Newton-type iterative method in order to calculate the equilibrium configuration at the end of the time step (Deng, 2014). Contrary to this, the dynamic analysis does not require the determination of the Jacobian matrix.

4. Elastic-plastic numerical simulations using the CP theory

The CPFEM simulations presented in this paper were carried out using the following open-source programs: NEPER as pre- and post- processor, and FEPX as the solver. The geometry of models is prepared in NEPER as a polycrystalline structure using the 3D Voronoi tessellation. The finite element mesh is generated in the same program. The numerical calculations are executed in FEPX program assuming proper boundary conditions. The stages of the CP analysis are shown in Fig. 3.

Simulations were done for cube and paddy-shape samples. Different number of grains and different meshes were tested. The generic copper alloy with a FCC crystalline structure with 12 slip systems was included here for which elastic and plastic parameters (FEPX, 2008) are contained in Table 1.

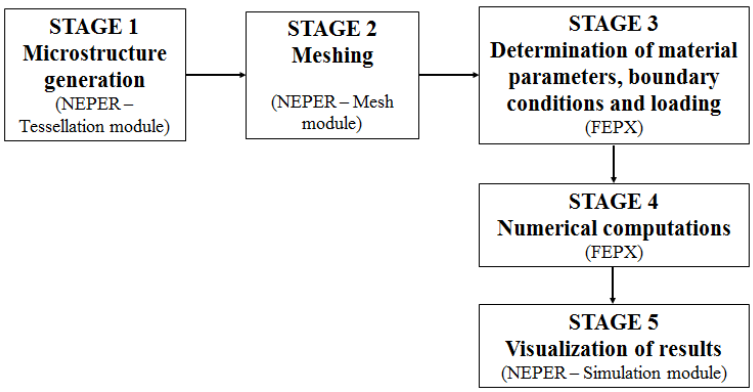

Fig. 3. Stages of CP analyses in NEPER and FEPX software

Table 1. Elastic parameters and other data associated with the strain hardening used in analyses

Parameter	Unit	Value
Elastic parameters		
Elastic constant C_{11}	MPa	$245{\cdot}10^3$
Elastic constant C_{12}	MPa	$155{\cdot}10^3$
Elastic constant C_{44}	MPa	$62.5{\cdot}10^3$
Plastic parameters		
material constant m	-	0.05
reference shear strain rate $\dot{\gamma}_0$	s^{-1}	1
fixed-state hardening rate scaling coefficient h_0	MPa	200
initial slip system strength g_0	MPa	210
initial slip system saturation strength g_{s0}	MPa	330
rate sensitivity coefficient k [-]	-	1

Although, the microstructural analyses of elastic-plastic problems using the CP theory give the better description of phenomena occurring in materials than the macroscopic ones, the computational cost of such calculations is very high.

In the further part of the research, the simple tension test of a plate with two holes is considered. The calculations are done in ABAQUS software using the user material procedure for the static analysis. The selected data applied in calculations are included in Table 2. On the basis of a macroscopic FEM analysis with the use of a UMAT, the information about stress and strain states, as well as, the deformation and velocity gradient tensors might be obtained. They can be then used in calculation based on the CP theory. So far, the UMAT material subroutine has been written for small strains only.

Table 2. Selected parameters used in the elastic-plastic analysis in ABAQUS

Parameter	Unit	Value
Young modulus E	MPa	$0.2 \cdot 10^5$
Poisson's ratio ν	-	0.33
Yield stress σ_p	MPa	200

5. Results

The CP analyses are usually done for a representative volume element (RVE) of a polycrystalline material in a cubic shape. Each grain in the RVE is considered as independent of other grains. The grain microstructure of the RVE might be represented by voxels with stair-stepped grain boundaries or using the smooth topology with a smooth flat grain boundaries (Fig. 4).

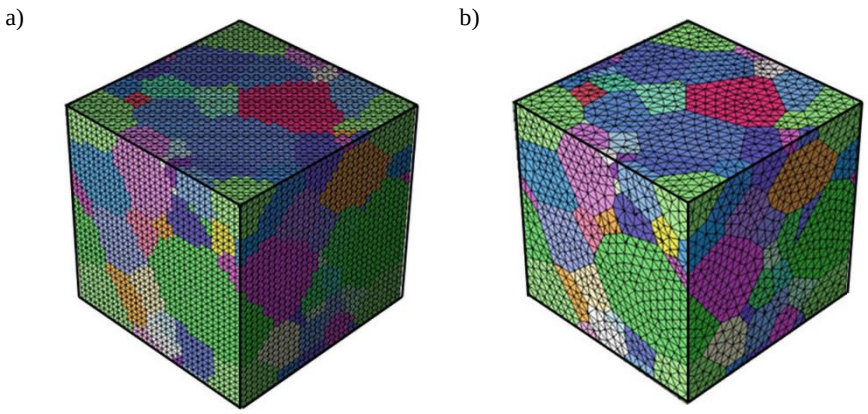

Fig. 4. The microstructure using a) the voxels and b) grains with a smooth topology

Some benchmark tests were conducted with NEPER and FEPX programs using the CP theory. In order to estimate the computation time, the non-isotropic polycrystalline sample of rectangular shape of dimensions 1 x 1 x 5 mm is subject to the tension with the strain rate $\dot{\varepsilon} = 0.02\ [\frac{1}{s}]$. The material is modelled as an aggregate of 200 single crystals with crystals random orientations defined by the Euler angles (Fig. 5). The grain size was in the range of 50-200 μm. Each grain is discretized by several tetrahedral elements (Fig. 6). All elements in the single grain have the same crystal orientations.

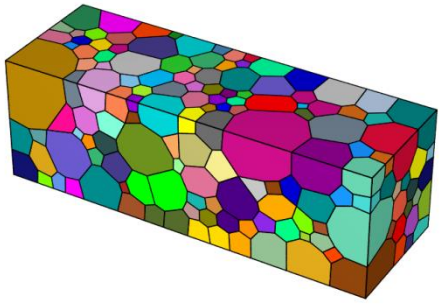

Fig. 5. The microstructure of a rectangular sample with 200 randomly orientated grains

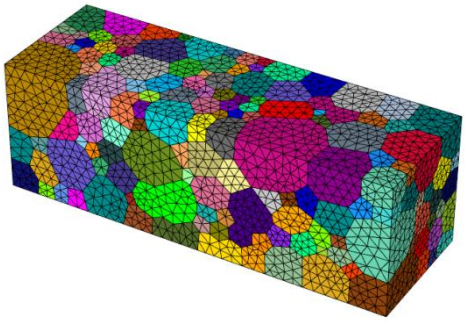

Fig. 6. FEM mesh for a rectangular sample with 200 grains

The σ_{zz} stress distribution acting on the loading direction is shown in Fig. 7. Heterogeneous distribution of stress inside the sample is noted, which is the result of grains anisotropy. The higher stress values in the range of 350-400 MPa are observed on the left and right faces. The heterogeneous stress distribution in the range of 50-200 MPa in the middle of a sample is also noted.

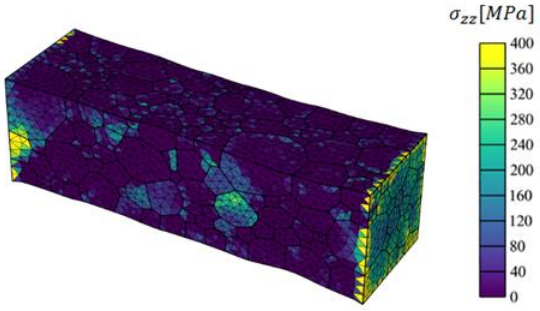

Fig. 7. Distribution of longitudinal σ_{zz} stress for a rectangular 200 grains sample

The distribution of strain in longitudinal direction ε_{zz} is presented in Fig. 8. The strain is mostly up to 0.006 and its distribution is heterogeneous. Some of grains show higher strains than others, which is associated with the anisotropy of the material.

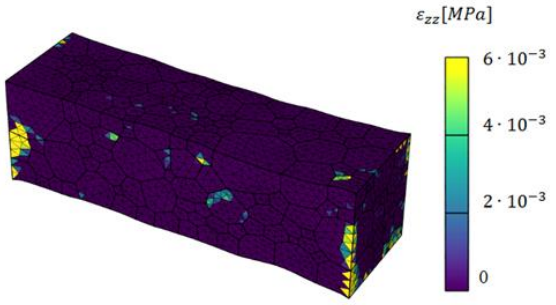

Fig. 8. Distribution of longitudinal strain ε_{zz} for a rectangular 200 grains sample

The microscopic analysis presented here allows predicting the macroscopic response of material. The macroscopic stress-stain curve for the tension test of rectangular sample with 200 grains was computed using the homogenization procedure (Fig. 9). The homogenized stress is computed as the total tensile force related to the actual cross-section (calculated with the assumption of the volume conservation).

In the second test a paddy shape sample with overall dimensions of 1.0 x 0.2 x 4.0 mm was subject to the tension load. The sample consists of 400 or 800 grains with random crystal orientations generated in the tessellation process (Fig. 10). The global coordinate system, material data, as well as, the boundary conditions are the same as in the previous test.

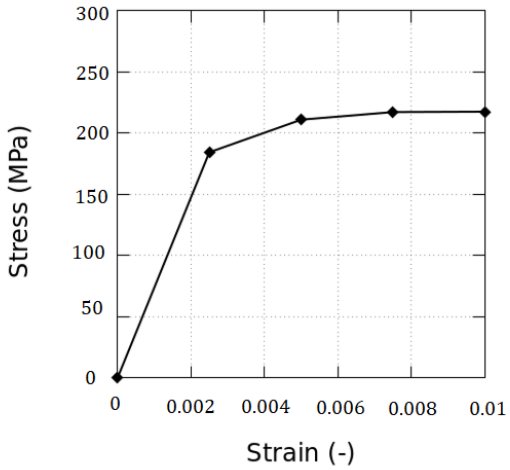

Fig. 9. Macroscopic stress-strain curve obtained with the use of the homogenization process

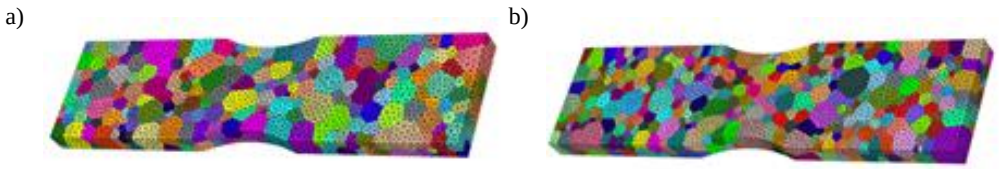

Fig. 10. The microstructure of a paddy-like shape; a) 400 and b) 800 grains

The effective stress and equivalent plastic strain distributions for the sample with 800 grains are presented in Fig. 11 and 12. The localization of strain near to the notch is noted. For both samples with different number of grains, shearing bands can be noted (contours sloped at 45˚ angle). The pole figures before and after the tensile load are presented in Fig. 13.

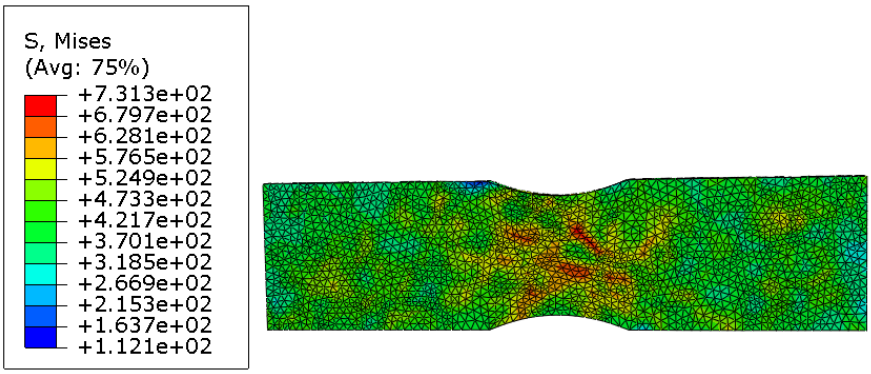

Fig. 11. The HMH (von Mises) stress distribution

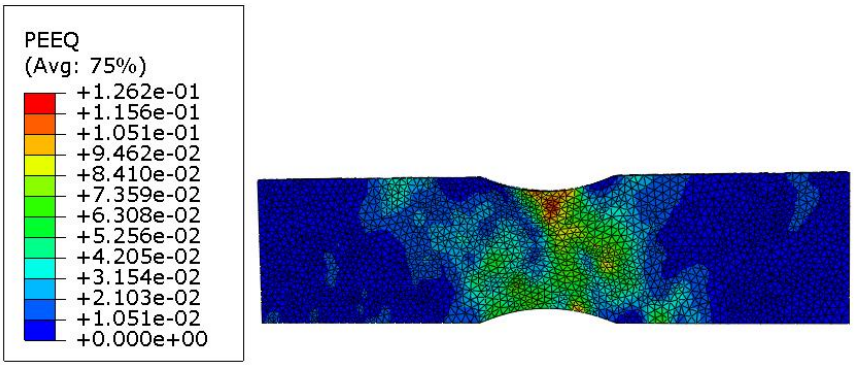

Fig. 12. The equivalent plastic strain (PEEQ) distribution

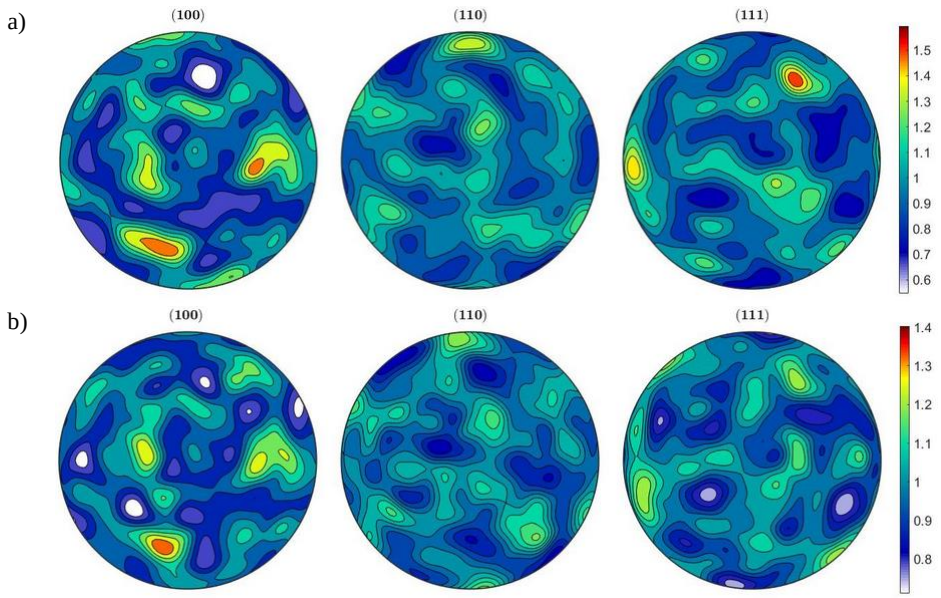

Fig. 13. Pole figures showing the microstructure of a copper alloy; a) before and b) after a tensile loading test

In the last test a flat plate with two holes fixed at one end is considered. The prescribed displacement is placed to the second end of this plate. The FE mesh consists of 1700 hexahedral elements (Fig. 14). The calculations are done as a static analysis for an isotropic material – all crystals have the same orientation. Using UMAT user material procedure developed for small displacements analysis, one can get stress and strain states, as well as, the velocity and deformation gradients, rotation tensors, etc.

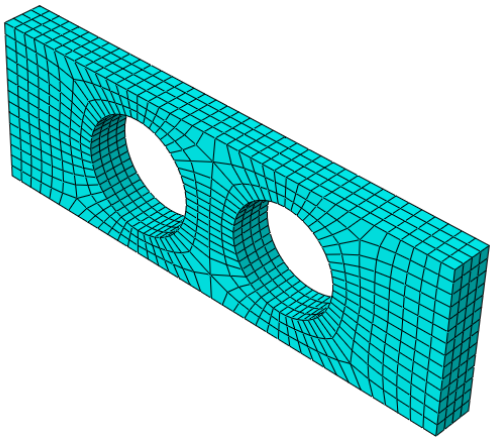

Fig. 14. The FEM mesh for plate with two holes example

The selected macroscopic results – the distribution of effective stress and the equivalent plastic strain are shown in Fig. 15. Because of the isotropic response of polycrystalline structure resulting from uniform crystal orientation, macroscopic stress and strain are coincident with the solution obtained within classical plasticity.

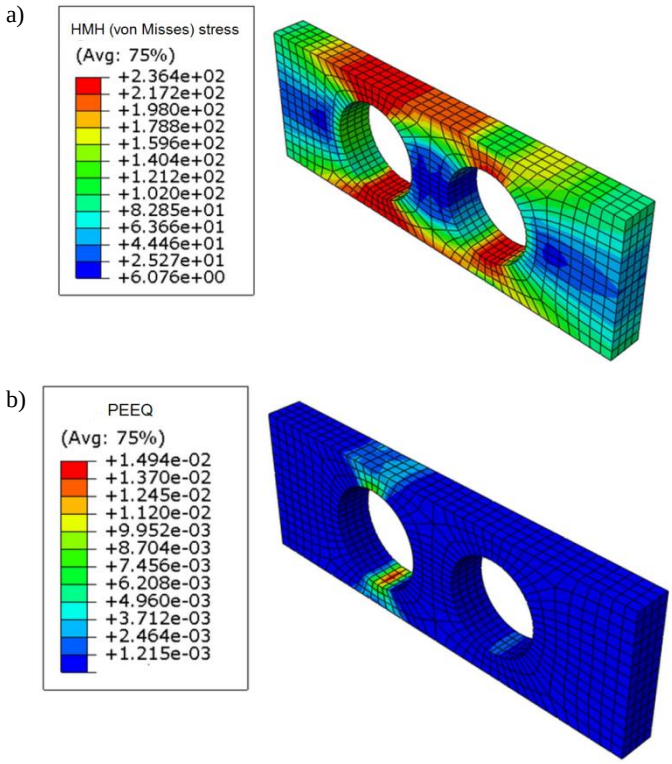

Fig. 15. The distribution of a) HMH (von Misses) stress and b) equivalent plastic strain in a plate with two holes

6. Discussion

Numerical tests presented in this paper show the potential of using crystal plasticity approach in solving elastic-plastic engineering problems. In this two-scale approach the macroscopic stress and strain are computed considering the dislocation slip as the source of the plastic deformation (Fig. 16).

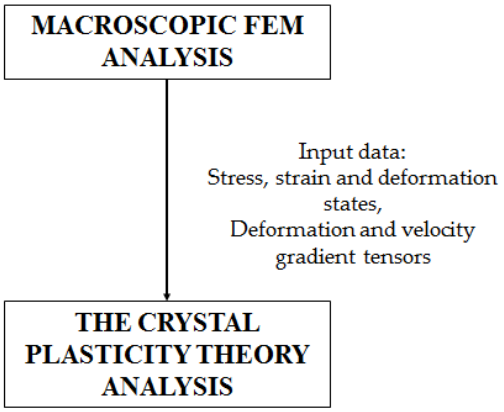

Fig. 16. The idea of the combined micro- and macromechanical analysis

The numerical CPFEM analysis is a complex and time-consuming. The following initial data are necessary for the microscopic analysis using the CPFEM model:

1) The elastic moduli of a material C_{ij}.
2) Number of potentially activated slip systems.
3) Initial crystallographic orientation in the sample coordinate system.
4) Shear strain rate which depends on the resolved shear stress.
5) Modulus of hardening.
6) Parameters for the iteration method.

The following steps of a combined micro- and macromechanical approach are used here:

1) Firstly, the orientation and slip systems are defined.
2) At the starting time of the increment, the information about stress, strain, rotation, time increment and solution dependent variable are necessary.
3) On the basis of the input parameters, the active slip systems and spin tensor are calculated.
4) After that, the slip normal and directions are determined.
5) The Jacobian matrix and other state variables are computed.
6) All the state variables and stress are updated at the end of the load increment.

The data obtained in numerical analyses using the CP theory shows anisotropic response of material under loading. Due to various orientation of crystals in polycrystalline materials the heterogeneous distribution of stress and strain is noted.

It is worth highlighting, that the user material subroutine UMAT used here should consider the rotation of the coordinate system. For this reason, the constitutive equations are written in the corotational frame. As a result of this objective stress rates should be used, namely Jaumann ($\boldsymbol{\sigma}^{\nabla J}$) and Green-Naghdi ($\boldsymbol{\sigma}^{\nabla G}$) stress (Eq. 39-40) (Okereke & Keates, 2018; Perez, 2017).

$$\boldsymbol{\sigma}^{\nabla J} = \dot{\boldsymbol{\sigma}} + \boldsymbol{\sigma}\boldsymbol{W} - \boldsymbol{W}\boldsymbol{\sigma} \tag{39}$$

$$\boldsymbol{\sigma}^{\nabla G} = \dot{\boldsymbol{\sigma}} + \boldsymbol{\sigma}\boldsymbol{\Omega} - \boldsymbol{\Omega}\boldsymbol{\sigma} \tag{40}$$

where: $\dot{\boldsymbol{\sigma}}$ is stress rate tensor in a corotational frame, $\boldsymbol{\sigma}$ is Cauchy stress tensor, $\boldsymbol{W}$ is spin tensor which comprises both the deformation and the rotation and $\boldsymbol{\Omega}$ is the angular velocity tensor resulting from a rigid body rotation. The parts $\boldsymbol{\sigma W}$ and $\boldsymbol{W\sigma}$ are associated with the rigid body rotation and the $\dot{\boldsymbol{\sigma}}$ term is associated with the material deformation (Wójcik & Skrzat, 2022c).

In ABAQUS program, the Jaumann stress rate is used for materials commercially implemented and for a user material subroutine. However, application of the Green-Naghdi stress rate can change the material response, especially for large shearing associated with the large rotations. It is possible to enforce using Green-Naghdi objective stress rate by adding two terms shown in Eq. 41.

$$\boldsymbol{\sigma}^{\nabla G} = \boldsymbol{\sigma}^{\nabla J} - \boldsymbol{\sigma}(\boldsymbol{W} - \boldsymbol{\Omega}) + (\boldsymbol{W} - \boldsymbol{\Omega})\boldsymbol{\sigma} \tag{41}$$

The rate-independent crystal plasticity approach based on dislocation slip as the only plastic response was used so far. In the further research the other models, e.g. viscoplastic ones will be considered and implemented in user material procedures. Further works will also focus on developing the VUMAT user material procedure for dynamic analyses. Other mechanisms of plastic deformations, e.g. the twinning phenomena will be also considered.

7. Summary and conclusions

The possibility of the use of a crystal plasticity (CP) theory to solve elastic-plastic problems is presented in this paper. The numerical calculations using the CP approach based on the Anand and Kothari model was done. The selected macro- and micro- scales software were applied here. The stress and plastic strain distributions within grains in the polycrystalline material were analyzed here. On the basis of results obtained, the main conclusions are as follows:

1) The CP theory gives the better interpretations of phenomena occurring in materials which are deformed plastically, especially in materials forming processes, e.g. SPD processes.
2) The numerical calculations on the microscale level are associated with the writing of a user material procedure which is a very time-consuming and difficult task.
3) The heterogeneous distribution of stress and strain in the polycrystalline material was noted which is a result of different orientation of crystals within grains. Some grains have higher stress and strain values than others, therefore.
4) In order to verify the correctness of the user material procedure written and results obtained, additional tests are necessary, e.g. shearing tests, equal channel angular processing (ECAP), extrusion test, etc.

Acknowledgments

This research has been supported by Slovak Research and Development Agency under the grant APVV-14-0834 “Zvýšenie kvality výstrižkov a efektívnosti strihania elektroplechov”.

References

Abdolvand, H., Daymond, M.R., & Mareau, C. (2011). Incorporation of twinning into a crystal plasticity finite element model: Evolution of lattice strains and texture in Zircaloy-2. *Int. J. Plast.*, *27*, 1721-1738. https://doi.org/10.1016/j.ijplas.2011.04.005

Acar, P., Ramazani, A., & Sundararaghavan, V. (2017). Crystal Plasticity Modeling and Experimental Validation with an Orientation Distribution Function for Ti-7Al Alloy. *Metals*, *7*, 459. https://doi.org/10.3390/met7110459

Alankar, A., Eisenlohr, P., & Raabe, D. (2011). A dislocation density-based crystal plasticity constitutive model for prismatic slip in α-titanium. *Acta Mater.*, *59*, 7003-7009. https://doi.org/10.1016/j.actamat.2011.07.053

Anand, L., & Kothari, M. (1996). A computational procedure for rate-independent crystal plasticity. *J. Mech. Phys. Solids*, *44*, 525-588. https://doi.org/10.1016/0022-5096(96)00001-4

Asaro, R.J., & Needleman, A. (1985). Texture development and strain hardening in rate dependent polycrystals. *Acta Metall.*, *33*, 923-953. https://doi.org/10.1016/0001-6160(85)90188-9

Balasubramanian, S., & Anand, L. (2002). Elasto-viscoplastic constitutive equations for polycrystalline fcc materials at low homologous temperatures. *J. Mech. Phys. Solids, 50(1),* 101-126. https://doi.org/10.1016/S0022-5096(01)00022-9

Bridier, F., McDowell, D.L., Villechaise, P., & Mendez, J. (2009). Crystal plasticity modeling of slip activity in Ti–6Al–4V under high cycle fatigue loading. *Int. J. Plast.*, *25*, 1066-1082. https://doi.org/10.1016/j.ijplas.2008.08.004

Buljak, V., Baivier-Romero, S., & Kallel, A. (2021). Calibration of Drucker–Prager Cap Constitutive Model for Ceramic Powder Compaction through Inverse Analysis. *Materials*, *14*, 4044. https://doi.org/10.3390/ma14144044

Chen, X., Jiao, R., & Kim, K.S. (2005). On the Ohno–Wang kinematic hardening rules for multiaxial ratcheting modeling of medium carbon steel. *Int. J. Plast.*, *21*, 161-184. https://doi.org/10.1016/j.ijplas.2004.05.005

Dabiri, M., Lindroos, M., Andersson, T., Afkhami, S., Laukkanen, A., & Björk, T. (2018). Utilizing the theory of critical distances in conjunction with crystal plasticity for low-cycle notch fatigue analysis of S960 MC high-strength steel. *Int. J. Fatigue*, *117*, 257-273. https://doi.org/10.1016/j.ijfatigue.2018.07.042

Deng, G. (2014). Crystal plasticity finite element method simulation of equal channel angular pressing. University of Wollongong Press.

Faul, U. (2021). Dislocation structure of deformed olivine single crystals from conventional EBSD maps. *Phys Chem Minerals*, *48*, 35. https://doi.org/10.1007/s00269-021-01157-3

FEPX: Finite Element Polycrystal Plasticity (2008). https://fepx.info

Frydrych, K., & Kowalczyk-Gajewska, K. (2016). A three-scale crystal plasticity model accounting for grain refinement in fcc metals subjected to severe plastic deformations. *Mater. Sci. Eng. A*, *658*, 490-502. https://doi.org/10.1016/j.msea.2016.01.101

Genna, F. (1993). Integration of plasticity equations for the case of Ziegler's kinematic hardening. *Comput. Methods Appl. Mech. Eng.*, *109*, 111-130. https://doi.org/10.1016/0045-7825(93)90227-O

Ibragimova, O., Brahme, A., Muhammad, W., Lévesque, J., & Inal, K. (2021). A new ANN based crystal plasticity model for FCC materials and its application to non-monotonic strain paths. *Int. J. Plast.*, 144, 103059. https://doi.org/10.1016/j.ijplas.2021.103059

Jeong, J., & Voyiadjis, G.Z. (2022). A physic-based crystal plasticity model for the prediction of the dislocation densities in micropillar compression. *J. Mech. Phys. Solids.*, 167, 105006. https://doi.org/10.1016/j.jmps.2022.105006

Khan, R., & Alfozan, A. (2019). Modeling of twinning-induced plasticity using crystal plasticity and thermodynamic framework. *Acta Mech.*, *230*, 2687-2715. https://doi.org/10.1007/s00707-019-02419-6

Khan, R., Pervez, T., Alfozan, A., Qamar, S.Z., & Mohsin, S. (2022). Numerical Modeling and Simulations of Twinning-Induced Plasticity Using Crystal Plasticity Finite Element Method. *Crystals*, *12*, 930. https://doi.org/10.3390/cryst12070930

Khan, R., Zahedi, F.I., & Siddiqui, A.K. (2016). Numerical Modeling of Twinning Induced Plasticity in Austenite Based Advanced High Strength Steels. *Procedia Manuf.*, *5*, 772-786. https://doi.org/10.1016/j.promfg.2016.08.063

Li, C., Cao, F., Chen, Y., Wang, H., & Dai, L. (2022). Crystal Plasticity Model Analysis of the Effect of Short-Range Order on Strength-Plasticity of Medium Entropy Alloys. *Metals*, *12*, 1757. https://doi.org/10.3390/met12101757

Li, H., Larsson, F., Colliander, M.H., & Ekh, M. (2021). Elastic-viscoplastic self-consistent modeling for finite deformation of polycrystalline materials. *Mater Sci Eng. A., 799,* 140325. https://doi.org/10.1016/j.msea.2020.140325

Li, Y.L., Kohar, C.P., Mishra, R.K., & Inal, K. (2020). A new crystal plasticity constitutive model for simulating precipitation-hardenable aluminum alloys. *Int. J. Plast.,* 132, 102759. https://doi.org/10.1016/j.ijplas.2020.102759

Liu, G., Mo, H., Wang, J., & Shen, Y. (2021). Coupled crystal plasticity finite element-phase field model with kinetics-controlled twinning mechanism for hexagonal metals. *Acta Mater., 202,* 399-416. https://doi.org/10.1016/j.actamat.2020.11.002

Men, M., & Meng, B. (2022). Crystal Plasticity Simulation of Yield Loci Evolution of SUS304 Foil. *Materials, 15,* 1140. https://doi.org/10.3390/ma15031140

Messner, M.C., Rhee, M., Arsenlis, A., & Barton, N.R. (2017). A crystal plasticity model for slip in hexagonal close packed metals based on discrete dislocation simulations. *Modelling Simul. Mater. Sci. Eng., 25,* 044001. https://doi.org/10.1088/1361-651X/aa687a

Mlikota, M., & Schmauder, S. (2018). On the Critical Resolved Shear Stress and Its Importance in the Fatigue Performance of Steels and Other Metals with Different Crystallographic Structures. *Metals, 8,* 883. https://doi.org/10.3390/met8110883

Nguyen, K., Zhang, M., Amores, V.J., Sanz, M.A., & Montáns, F.J. (2021). Computational Modeling of Dislocation Slip Mechanisms in Crystal Plasticity: A Short Review. *Crystals, 11,* 42. https://doi.org/10.3390/cryst11010042

Nibur, K.A., & Bahr, D.F. (2003). Identifying slip systems around indentations in FCC metals. *Comput. Mater. Sci., 49,* 1055-1060. https://doi.org/10.1016/j.scriptamat.2003.08.021

Okereke, M., & Keates, S. (2018). Finite Element Applications. A Practical Guide to the FEM Process. Springer.

Paudel, Y., Giri, D., Priddy, M.W., Barrett, C.D., Inal, K., Tschopp, M.A., Rhee, H., & El Kadiri, H. (2021). A Review on Capturing Twin Nucleation in Crystal Plasticity for Hexagonal Metals. *Metals, 11,* 1373. https://doi.org/10.3390/met11091373

Perez, N. (2017). Theory of Elasticity. Springer.

Pramanik, S., Tasche, L., Hoyer, K.P., & Schaper, M. (2021). Correlation between Taylor Model Prediction and Transmission Electron Microscopy-Based Microstructural Investigations of *Quasi*-In Situ Tensile Deformation of Additively Manufactured FeCo Alloy. *J. Mater. Eng. Perform., 30,* 8048–8056. https://doi.org/10.1007/s11665-021-06065-9

Ramos, P.M., Herranz, M., Foteinopoulou, K., Karayiannis, N.Ch., & Laso, M. (2020). Identification of Local Structure in 2-D and 3-D Atomic Systems through Crystallographic Analysis. *Crystals, 10,* 1008. https://doi.org/10.3390/cryst10111008

Remache, D., Semaan, M., Rossi, J.M., Pithioux, M., & Milan, J.L. (2020). Application of the Johnson-Cook plasticity model in the finite element simulations of the nanoindentation of the cortical bone. *J. Mech. Behav. Biomed. Mater., 101,* 103426. https://doi.org/10.1016/j.jmbbm.2019.103426

Romanova, V., Balokhonov, R., Zinovieva, O., Lychagin, D., Emelianova, E., & Dymnich, E. (2022). Mechanical Aspects of Nonhomogeneous Deformation of Aluminum Single Crystals under Compression along [100] and [110] Directions. *Metals, 12,* 397. https://doi.org/10.3390/met12030397

Ryś, M., Stupkiewicz, S., & Petryk, H. (2022). Micropolar regularization of crystal plasticity with the gradient-enhanced incremental hardening law. *Int. J. Plast., 156,* 103355. https://doi.org/10.1016/j.ijplas.2022.103355

Sajjad, H.M., Hanke, S., Güler, S., ul Hassan, H., Fischer, A., & Hartmaier, A. (2019). Modelling Cyclic Behaviour of Martensitic Steel with J2 Plasticity and Crystal Plasticity. *Materials, 12,* 1767. https://doi.org/10.3390/ma12111767

Schäfer, B.J., Song, X., Sonnweber-Ribic, P., ul Hassan, H., & Hartmaier, A. (2019). Micromechanical Modelling of the Cyclic Deformation Behavior of Martensitic SAE 4150—A Comparison of Different Kinematic Hardening Models. *Metals, 9,* 368. https://doi.org/10.3390/met9030368

Sundararaghavan, V., & Zabaras, N. (2008). A multi-length scale sensitivity analysis for the control of texture-dependent properties in deformation processing. *Int. J. Plast., 24,* 1581–1605. https://doi.org/10.1016/j.ijplas.2007.12.005

Weinberger, C.R., Boyce, B.L., & Battaile, C.C. (2013). Slip planes in bcc transition metals. *Int. Mater. Rev., 58,* 296-314. https://doi.org/10.1179/1743280412Y.0000000015

Wójcik, M., & Skrzat, A. (2020). Fuzzy logic enhancement of material hardening parameters obtained from tension–compression test. *Continuum Mech. Thermodyn., 32,* 959-969. https://doi.org/10.1007/s00161-019-00805-y

Wójcik, M., & Skrzat, A. (2021). The Coupled Eulerian-Lagrangian Analysis of the KOBO Extrusion Process. *ASTRJ, 15,* 197-208. https://doi.org/10.12913/22998624/131663

Wójcik, M., & Skrzat, A. (2022a). An Elastic-Plastic Analysis of Polycrystalline Structure Using Crystal Plasticity Modelling – Theory and Benchmark Tests. *ASTRJ, 16,* 163-177. https://doi.org/10.12913/22998624/154025

Wójcik, M., & Skrzat, A. (2022b). Coupled Thermomechanical Eulerian-Lagrangian Analysis of the KOBO Extrusion Process. *Arch. Metall. Mater., 67,* 1185-1193. https://doi.org/10.24425/amm.2022.139719

Wójcik, M., & Skrzat, A. (2022c). Numerical modelling of the KOBO extrusion process using the Bodner–Partom material model. *Meccanica*, *57*, 2213–2230. https://doi.org/10.1007/s11012-022-01569-7

Yaghoobi, M., Ganesan, G., Sundar, S., Lakshmanam, A., Rudraraju, S., Allison, J.E., & Sundararaghavan, V. (2019). PRISMS-Plasticity: An open-source crystal plasticity finite element software. *Comput. Mater. Sci.*, *169*, 109078. https://doi.org/10.1016/j.commatsci.2019.109078

Yang, G., & Park, S.-J. (2003). Deformation of Single Crystals, Polycrystalline Materials, and Thin Films: A Review. *Materials*, *12*, 2003. https://doi.org/10.3390/ma12122003

Yang, G., Dayong, A., Fengbo, H., Liu, X., Guozheng, K., & Xu, Z. (2022). Multiple-mechanism and microstructure-based crystal plasticity modeling for cyclic shear deformation of TRIP steel. *Int. J. Mech. Sci*., 222, 107269. https://doi.org/10.1016/j.ijmecsci.2022.107269

Sprężysto-plastyczne Analizy Numeryczne Niezależne od Prędkości Odkształcenia dla Materiałów Polikrystalicznych z Zastosowaniem Teorii Plastyczności Kryształów

Streszczenie

Analizy makroskopowe procesów przeróbki plastycznej prezentują jedynie ogólny zarys rozważanego problemu, bez uwzględnienia mechanizmów odkształcenia plastycznego oraz ewolucji mikrostruktury. W celu rozważania procesów przeróbki plastycznej stosowane są symulacje numeryczne w ramach teorii plastyczności kryształów uwzgledniające zmianę tekstury, anizotropię oraz umocnienie odkształceniowe. W artykule zaprezentowano zastosowanie modelu Ananda i Kothari w ramach teorii plastyczności kryształów niezależnej od prędkości odkształcenia do rozwiązywania analiz numerycznych dla materiałów polikrystalicznych. W badaniach uwzględniono poślizg dyslokacyjny jako główny mechanizm odkształcenia plastycznego. Zaprezentowano wybrane rezultaty dla problemów sprężysto-plastycznych uzyskane zarówno w skali makro, jak i mikro- dla całkowania typu *explicit* i *implicit*. Uzyskano niejednorodny rozkład naprężenia i odkształcenia w poszczególnych ziarnach, związany z różną orientacją kryształów. Modelowanie numeryczne z zastosowaniem teorii plastyczności kryształów dla materiałów poddanych plastycznemu odkształceniu dostarcza nie tylko informacje o zmianie kształtu materiału w skali makro, ale także opisuje zjawiska zachodzące w materiale w skali mikro-.

Słowa kluczowe: plastyczność kryształów, materiał polikrystaliczny, odkształcenie plastyczne, CPFEM, poślizg dyslokacyjny